PERGAMON

Journal of Structural Geology 24 (2002) 469–483

JOURNAL OF STRUCTURAL GEOLOGY

www.elsevier.com/locate/jstrugeo

The development of contrasting structures during the cooling and crystallisation of a syn-kinematic pluton

M.J. Pawley*, W.J. Collins

Discipline of Geology, University of Newcastle, Callaghan, NSW 2308, Australia

Received 9 June 2000; revised 2 March 2001; accepted 5 March 2001

Abstract

Structural elements of a syn-kinematic pluton in the Pilbara Craton of Western Australia reflect evolving rheology during progressive crystallisation, representing a transition from magmatic, through high-temperature sub-solidus to low-temperature deformation. Magmatic elements include: (1) NNE-trending, sub-vertical, kilometre-scale folds (outlined by xenolith trains) that have a magmatic axial planar foliation defined by aligned K-feldspar, (2) cross-cutting, ENE-trending, sub-vertical shear zones intruded by numerous ≤metre-scale granite sheets, and (3) a narrow, concordant magmatic K-feldspar foliation in the granite host-rock adjacent to the shear zones. Microstructures, such as fractured feldspars healed by quartz that is continuous with matrix grains, further suggest that deformation occurred while the pluton was magmatic. High-temperature structural elements include 'checkerboard' sub-grain boundaries in quartz, whereas deformation at lower temperatures is indicated by kinked feldspar, recrystallised microcline and undulose quartz. A NNE-trending, sub-vertical sub-solidus foliation, defined by elongate quartz aggregates, overprints all the above mentioned features. Generation of these sequential structural elements correspond to the transition from Newtonian-fluid, through Bingham-type, to Newtonian-solid behaviour as the crystal fraction of the felsic magma increased. The orientation of the structures is consistent with a regional ESE–WNW shortening direction throughout magma crystallisation. This study indicates how evolving magma rheology and regional strain regimes control the micro- to macro-structural elements of a syn-tectonic pluton.

Keywords: Crystallising magma; Foliation; Rheology; Shearing

1. Introduction

Crystallisation of a magma represents a transition from liquid (±solids) to a solid crystalline rock, during which the magma undergoes progressively different rheological states, each with characteristic behaviour. At low crystal fractions the magma behaves as a Newtonian liquid with no yield strength, and a linear relation between an applied stress and strain rate. As the crystal fraction increases, increased grain interaction will cause the magma to behave as a non-Newtonian fluid, with a non-linear relation between viscosity and strain rate (Smith, 1997). The magma acts as a fluid until strain rate or fluid pressure (P_f) is increased, resulting in transient high viscosity (i.e. shear thickening). Finally, at high crystal fractions the magma behaves as a Newtonian solid because the crystals form a closely packed network (Fernandez and Barbarin, 1991; Vigneresse et al., 1996). Consequently, a magma body does not behave uniformly as the crystal fraction increases during cooling, particularly if it is subjected to either near- or far-field differential stress.

The rheological state influences the processes that can act during the crystallisation of a syn-kinematic magma (e.g. shearing, melt segregation, foliation development, microstructural evolution). Deformation may be partitioned into, or initiate within, crystallising magmas since they are rheologically weaker than the solid host rock (i.e. magma-enhanced strain localisation; Vauchez et al., 1997; McCaffrey et al., 1999). During partial melting, the melt may increase fluid pressure (P_f) and initiate or focus deformation by lowering the effective stress in a body. This facilitates failure processes, such as 'melt-enhanced embrittlement', where fracturing occurs within relatively rigid or partially melted rocks (Hollister and Crawford, 1986; Davidson et al., 1994; Brown and Solar, 1998). Several studies have also examined how the orientation of shear zones relative to the shortening direction may be influenced by evolving rheology as the crystal fraction increased (e.g. McCaffrey, 1994; Buttner, 1999).

Strain acting on the crystallising magma may affect the segregation and transfer of residual liquid, as the crystal

* Corresponding author. Tel.: +61-2-4921-5404; fax: +61-2-4921-6925.
E-mail address: mark.pawley@newcastle.edu.au (M.J. Pawley).

0191-8141/02/$ - see front matter
PII: S0191-8141(01)00069-4

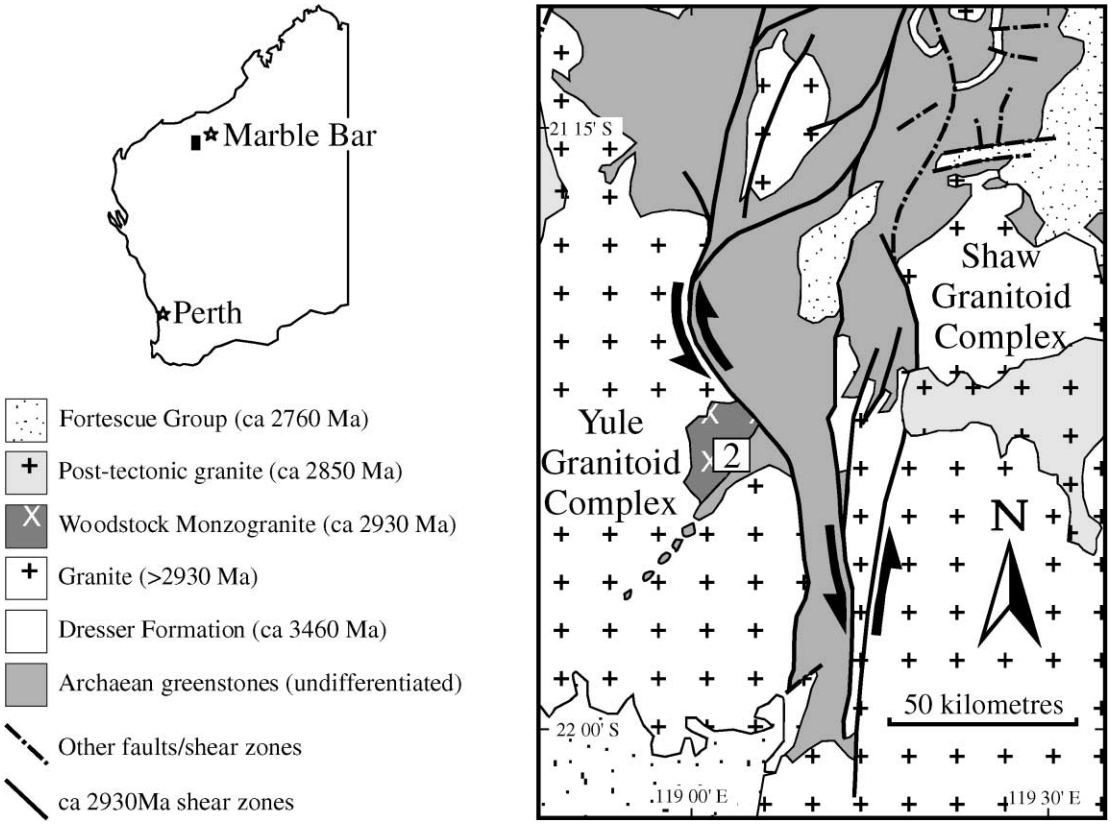

Fig. 1. Simplified geological map of the eastern Pilbara craton, to show the area around the southern MSZ/LWSC that comprises the ~2930 Ma shears. Inset shows the location of the map in Western Australia. '2' represents the area of Fig. 2.

network may still be permeable and permit fluid flow (Vigneresse et al., 1996). Matrix compaction during deformation may increase the pore pressure, generating P_f gradients over short distances and significantly enhancing fluid flow. The melt will flow through the deformable matrix at the grain-scale, concentrating in veinlets where further segregation occurs (Rutter, 1997). This process of melt segregation is similar to that proposed for partially melted rocks (Sawyer, 1994, 1996). Subsequent distribution of segregated melt is often structurally controlled by lower pressure sinks, such as shear zones, dilational fractures and pre-existing foliations (Pitcher and Berger, 1972; Mahood and Cornejo, 1992; John and Stunitz, 1997; Smith, 1997). The concentration of segregated melt in shear zones and fractures is also supported by experimental work (e.g. Rutter and Neumann, 1995; Grujic and Mancktelow, 1998; Rosenberg and Handy, 2000). Segregation of melt can also influence magma composition, as the removal of interstitial liquids from the crystal cumulate might result in differentiation within a crystallising magma (e.g. Mahood and Cornejo, 1992).

Several studies have described the transition of microstructures in syn-kinematic magmas from magmatic, through high temperature (sub-solidus) to lower temperature textures (Paterson et al., 1989; Miller and Paterson, 1994; Tribe and D'Lemos, 1996; Schofield and D'Lemos, 1998). Syn-kinematic magmatic foliations are typically defined by the alignment and tiling of elongate igneous minerals and enclaves (Blumenfeld and Bouchez, 1988; Paterson et al., 1989; Miller and Paterson, 1994; Pons et al., 1995), while at greater crystal fractions, grains can mechanically interact and be fractured, with the fracture healed by magmatic minerals. The magmatic foliation may also be disturbed by oblique dilational shear zones, which may possess their own magmatic foliation (Pons et al., 1995; Smith, 1997). As the temperature falls below the solidus, deformation is characterised by initially plastic flow then later brittle failure of minerals (Passchier and Trouw, 1996).

The syn-kinematic Woodstock Monzogranite, in the Pilbara Craton of Western Australia, preserves a range of structural elements and textures that developed during the deformation of a crystallising pluton. The pluton was emplaced and deformed during regional, bulk transpression (Van Kranendonk and Collins, 1998; Zegers et al., 1998), which places a control on the strain regime during its cooling and crystallisation. This framework allows the relation between structural development and evolving rheology to be examined.

2. Regional geology

The eastern Pilbara Craton of Western Australia is an

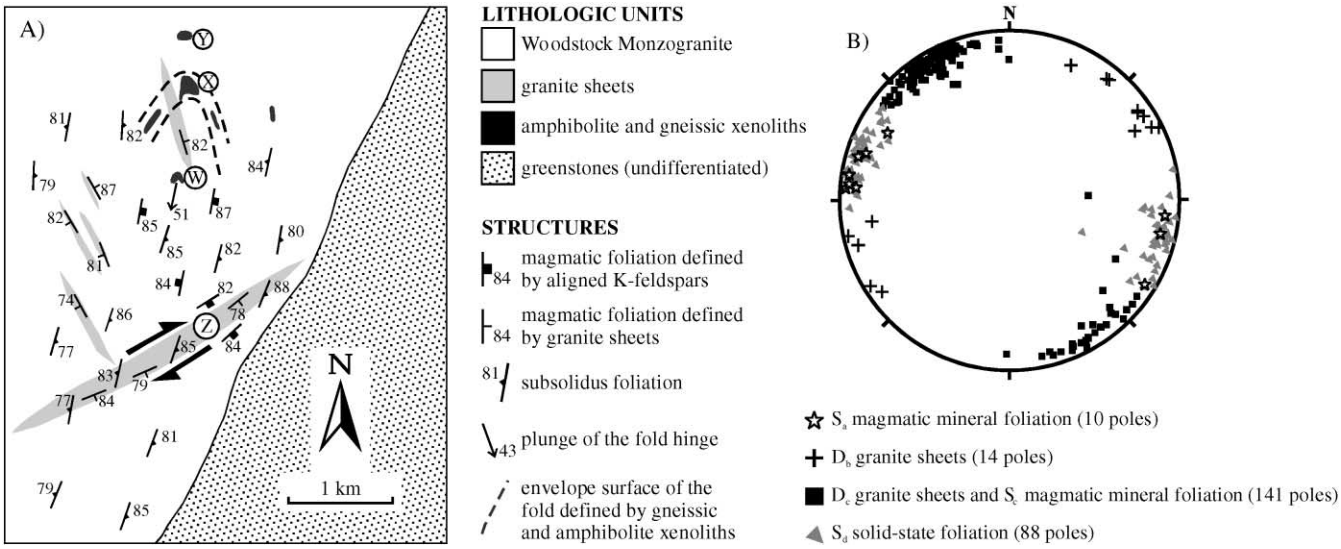

Fig. 2. (A) Geological map of the eastern Woodstock Monzogranite showing representative structural data, the location of the larger supracrustal rafts and the distribution of the granite sheets. 'W–Z' indicate the locations of outcrops described in the text. (B) Stereoplot of structural data from the eastern Woodstock pluton.

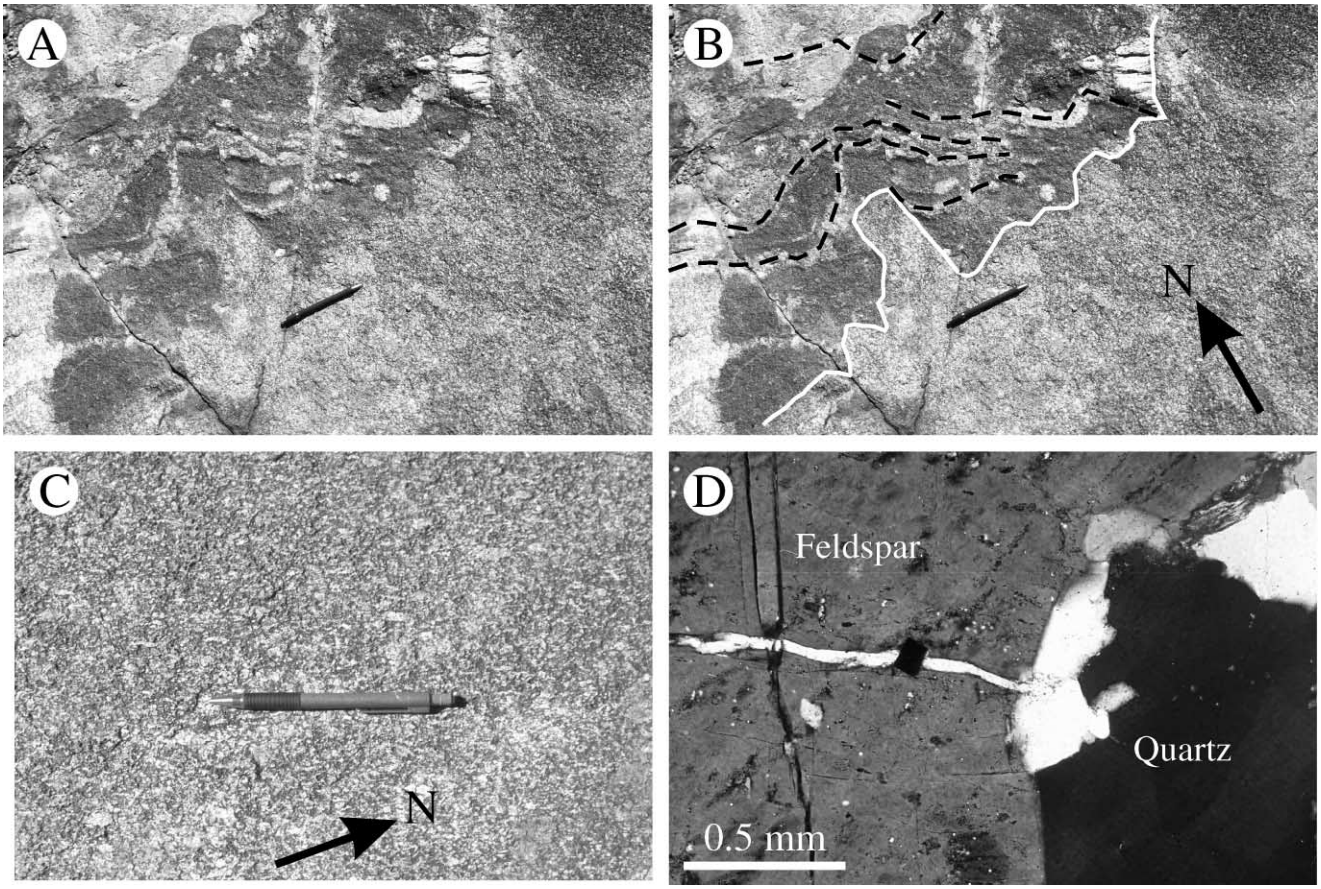

Fig. 3. (A) Photograph of a pavement, showing the Woodstock Monzogranite (right side of photograph) that intruded the axial plane of a meso-scale fold within a gneissic xenolith. (B) Same photograph as (A), with the white line showing the contact between the monzogranite and the gneiss, and the black dashed line showing the trend of leucosomes within the gneiss. (C) Photograph of a pavement, to show the NNE-trending D_a feldspar alignment (parallel to the pencil) in the Woodstock Monzogranite (the arrow points north). (D) Photomicrograph (crossed polarised light) to show a fracture in a feldspar phenocryst filled by quartz that is optically continuous with the external quartz grain.

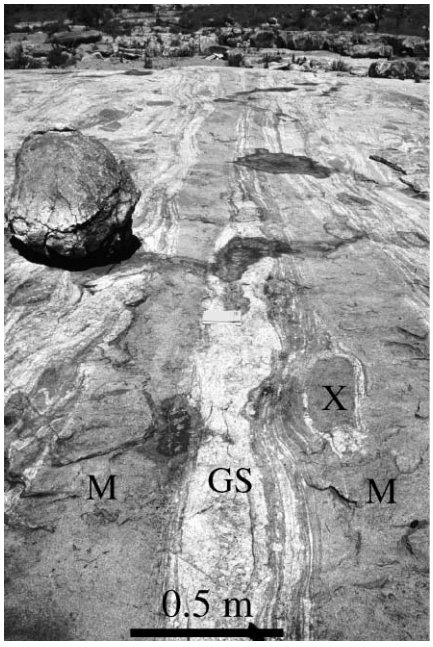

Fig. 4. NNW-trending D_b layered granite sheets in the northwest Woodstock pluton. The darker layers (M) are Woodstock Monzogranite, the layer 'GS' comprises granite sheets and block 'X' is a gneissic xenolith. View is to the SSE.

Archaean granite greenstone terrane with greenstone synclines surrounding large (~60 km diameter), intrusive, multiphase granite domes. The greenstone sequences formed by periodic basalt-dominated volcanism and minor clastic sedimentation that occurred between 3515 and 2760 Ma (Hickman, 1983; Thorpe et al., 1992; Buick et al., 1995). The granitoid domes have a similar punctuated history with magmatism occurring approximately coeval with volcanism at ca. 3450, ca. 3410, ca. 3300–3200, ca. 2930 and ca. 2850 Ma (Bickle et al., 1989; Williams and Collins, 1990; Bickle et al., 1993; Nelson, 1998).

The dome and basin pattern of the eastern Pilbara Craton was established by ca. 2930 Ma, when the region underwent NW–SE-directed compression (Van Kranendonk and Collins, 1998). The Shaw Granitoid Complex was displaced northward relative to the Yule Granitoid Complex along a series of craton-scale, curvilinear, sinistral, transpressional shear zones (Fig. 1), called the Mulgandinnah Shear Zone/Lalla Rookh–Western Shaw Structural Corridor (MSZ/LWSC; Van Kranendonk, 1998; Van Kranendonk and Collins, 1998; Zegers et al., 1998) dated by U–Pb SHRIMP analysis of zircon at 2934 ± 2 Ma (Zegers, 1996). Lineations in the MSZ/LWSC are sub-horizontal, suggesting predominantly strike-slip displacement.

Within the granite domes, deformation is represented by ~kilometre-scale, dextral shear zones that consistently strike ~070° and a penetrative ~NNE trending sub-solidus foliation. The ca. 2930 Ma deformation event was coeval with emplacement of felsic magmas into the Yule and Shaw Granitoid Complexes. These include the Woodstock Monzogranite (Fig. 1), a ~400 km^2 pluton that intruded the eastern margin of the Yule Batholith, adjacent to the MSZ/LWSC, at 2927 ± 3 Ma (SHRIMP age; Nelson, 1998). This pluton is the focus of this paper.

3. Field observations

Four foliations have been recognised in the Woodstock pluton. Regional mapping and overprinting relations indicate that they can be assigned a temporal order. However, as discussed below, all appear to relate to varying stages of crystallisation in the pluton and thus are assigned a–d, rather than 1–4.

Detailed mapping in the eastern Woodstock pluton revealed trains of <100-m-scale orthogneiss and supracrustal rafts (typically amphibolite with quartzite interbeds) that define a kilometre-scale, upright, south plunging, close F_a synform (Fig. 2). The rafts have sharp margins, with the granite truncating the leucosomes in the migmatitic orthogneisses. Several of the rafts have also been folded.

At outcrop W (Fig. 2), a ~100-m-scale amphibolite raft in the granite is folded into a F_a synform that plunges moderately to the south (51 → 192°), while metre-scale, elongate amphibolite xenoliths adjacent to the raft are consistently aligned with a similar plunge (50 → 190°). Biotite schlieren are aligned axial planar to the folds and trend sub-vertically at 020°, and are defined as S_a. Further north (locality X in Fig. 2), a raft of migmatitic orthogneiss has been openly folded. The axial planes of <metre-scale F_a folds at the raft margin trend ~N–S, and have been intruded by the Woodstock Monzogranite, which also cuts folded orthogneiss leucosomes (Fig. 3A and B). Approximately 500 m further north (location Y in Fig. 2), a folded amphibolite raft is cut by a metre-wide dyke of the monzogranite, which is concordant with the F_a axial plane.

Throughout the eastern Woodstock pluton, a pervasive sub-vertical, NNE-trending foliation is sub-parallel to the axial plane of the kilometre-scale synform (Fig. 2A), and therefore is assigned S_a. It is defined by the preferred alignment of euhedral to subhedral K-feldspar phenocrysts (Figs. 2B and 3C), which are locally fractured and filled with quartz that is optically continuous with external grains in the matrix (Fig. 3D). Therefore, we interpret the pervasive S_a foliation, and its associated F_a folds, to have formed in the magmatic state.

Cross-cutting D_a structures in two main directions (NNW and ENE; Fig. 2) are zones of centimetre- to metre-scale granite sheets (Fig. 4). In each zone, hundreds to thousands of individual sheets are composed of heterogeneous leucogranite and biotite-rich schlieren. Some sheets contain equant to tabular, metre-scale orthogneiss xenoliths, but they are rare. The NNW-trending sheets are semi-continuous over tens of metres, whereas the ENE variety can be mapped for >100 m, even if only centimetre-scale wide. All sheets have typical granitic textures, characterised by

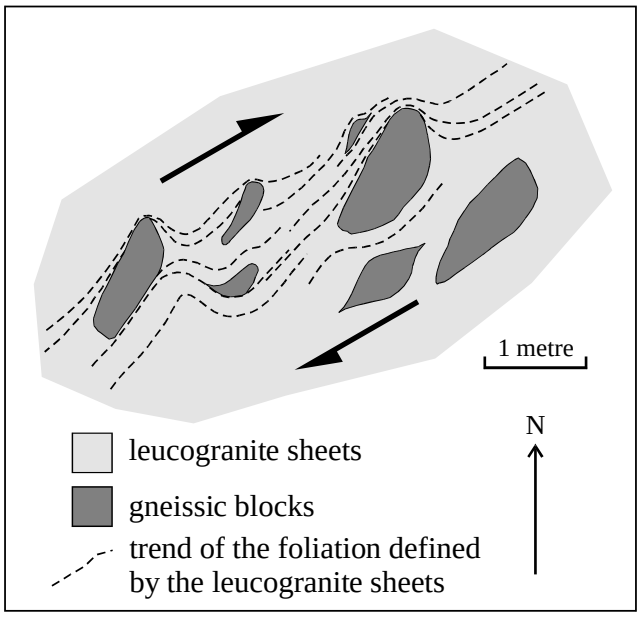

Fig. 5. Diagram of the oblique, metre-scale gneissic blocks that form a xenolith train within the ENE-trending D_c granite sheets. Note the consistent angular relation between the blocks and granite layers.

interlocking feldspar and dispersed, non-aligned biotite. The NNW-trending zones are cut by the ENE-trending zones on a regional scale and are therefore assigned as D_b, and the latter as D_c.

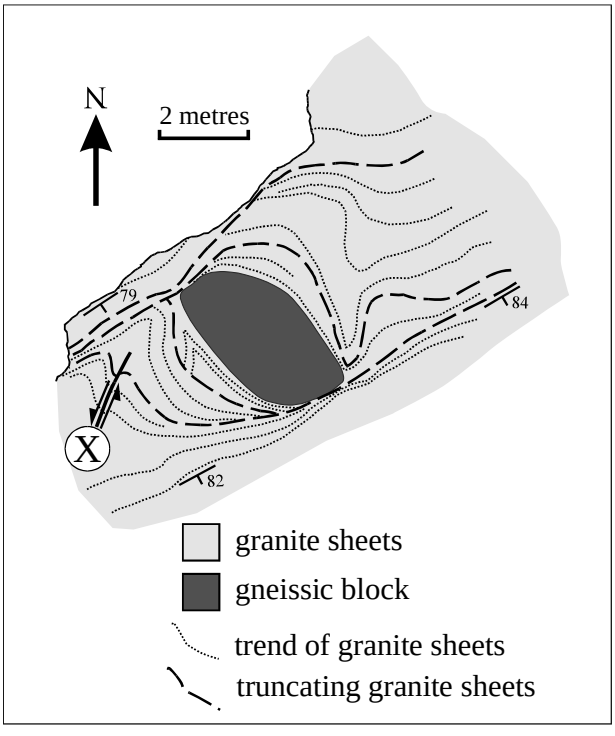

Fig. 6. Diagram of a gneissic block that has been 'wrapped' by granitic sheets during apparent clockwise rotation. The diagram shows the folds in the inner sheets that were truncated by the outer sheets, which were also folded. X is the sinistral shear zone described in the text.

The D_b sheeted granites form sub-vertical, <100-m-wide, 1-km-long zones (Fig. 2A) that contain metre-scale, parallel layers of homogenous monzogranite, texturally similar to the monzogranite host (Fig. 4). The margins of the layers exhibit pinch and swell structures (Fig. 4), and they taper to millimetre-width, discontinous veinlets. The sheets contain metre-scale gneissic xenoliths that are generally equant and do not exhibit a consistent asymmetry.

The D_c granite sheets are confined to a ~3-km-long, ~300-m-wide sub-vertical zone that cuts through the southern part of the pluton (Fig. 2). A large exposure ($300 \times 350\ m^2$) of the zone (locality Z in Fig. 2) reveals markedly different orthogneiss xenolith geometries, which provide information on the nature and significance of the granite sheets, as discussed below.

At locality Z (Fig. 2), gneissic xenoliths are typically elongate and arranged in trains that can be traced along strike for >100 m. Individual xenoliths in one such train are consistently aligned ~40° oblique to the sheets, having an imbrication pattern (Fig. 5). The enveloping centimetre-scale granite sheets are consistently thinner against the northwest side of the xenoliths, but rapidly thicken between these blocks. Some sheets terminate against the larger blocks, but reappear on the other side. In addition, the sheets form an undulatory pattern of asymmetric fold-like structures around the xenoliths. No axial planar foliation is associated with these fold-like structures, nor any mineral alignment parallel to the sheets themselves. This indicates that no strain was recorded during development of these structures.

Twenty metres northward, a $4 \times 2\ m^2$ gneissic xenolith has a spiral-like geometry (Fig. 6). The innermost granite sheets are tightly folded with an inner limb parallel to the gneissic block. The outer fold limbs are irregular, with those on the southeast side of the block opening out parallel to the ENE structural trend of the outcrop. In contrast, the granite sheets on the southwest side of the block have been truncated by outer sheets, which were subsequently truncated by the outermost sheets (Fig. 6). A metre-scale, sinistral shear zone has developed within the granite sheets west of the xenolith (X in Fig. 6). It contains a non-foliated concordant granite vein that is aligned sub-parallel to the axial plane of the adjacent fold in the spiral. Apart from this minor shear zone, no axial planar foliation is associated with the folds.

Approximately 50 m away, an ~20-m-thick monzogranite layer, with biotite schlieren, contains a metre-scale equant gneissic xenolith that has a ~4-m-long 'tail' of heterogeneous, centimetre-scale leucogranite sheets (Fig. 7). The granite sheets are thinnest at the eastern side of the xenolith, then increase in thickness around the block, before tapering off into the monzogranite host to form the southwest projecting tail (Fig. 7). The sheets, although irregular, are relatively symmetrical, are sub-parallel to the ENE structural trend of the outcrop, but show no internal mineral alignment. The whole structure resembles a 'comet'.

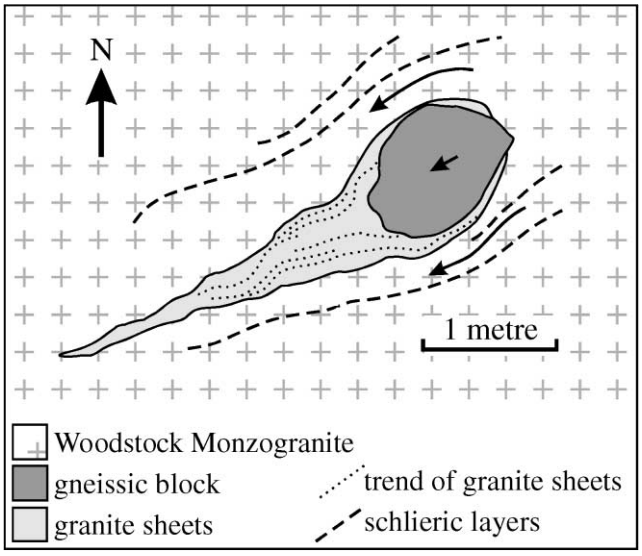

Fig. 7. Diagram of the gneissic block in the Woodstock Monzogranite that possesses a symmetrical tail of granitic sheets on one side. The length of the arrows are proportional to the apparent velocities of the block and its host magma.

The contact between the monzogranite layer and adjacent granite sheets is cut by a discontinuous, leucocratic, coarse-grained dyke (Fig. 8). The dyke is tapered and forms a funnel-shaped intrusion that is widest in the monzogranite, where it projects for <1 m. In the monzogranite, the margins of the dyke are diffuse and schlieric layering adjacent to the end of the dyke is convex towards the contact. The dyke has a sharp margin and can be traced for several metres in the granite sheets.

Beyond the D_c zone at locality Z (Fig. 2), the host monzogranite contains two foliations, each defined by the alignment of euhedral to subhedral K-feldspar phenocrysts. The dominant foliation, defined by $\leq$1-cm-long 'matrix' K-feldspars, is sub-vertical and trends ENE, sub-parallel to the granite sheets. A subordinate foliation, defined by ~5-cm-long feldspars (Fig. 9), trends NNE and is aligned 40° oblique to the general ENE trend of the layers, concordant with the imbricated blocks in the sheeted granite. Like the imbrication pattern of the asymmetric xenoliths in the granite sheets, schlieren asymmetrically envelope the large feldspars. Thinnest and warped against the western side, the schlieren curls around the ends of the phenocrysts, before continuing in the general ENE-trend (Fig. 9). The consistent asymmetry of the two foliations resembles that of *S*/*C* fabrics in mylonitic rocks.

Another well-developed pervasive foliation, which is defined by elongate, recrystallised, centimetre-scale quartz aggregates (Figs. 3C and 9), overprints the D_b and D_c structures and therefore is assigned to D_d. It trends sub-vertically ~NNE (Fig. 2), sub-parallel to the axial planar parallel S_a foliation (Fig. 2B). If this foliation did not overprint the sheeted granites (S_b and S_c) it could easily be interpreted as the late-stage manifestation of S_a, which is defined by dimensional alignment of K-feldspar.

Within the granite sheets and host monzogranite, a range of microstructures provide evidence for deformation during cooling of the pluton. They contain patches of interlocking, subhedral (often perthitic) feldspars that are surrounded by interstitial, randomly oriented biotite blades. Quartz preserves 'checkerboard' sub-grain boundaries indicating basal ($\langle c \rangle$) and prismatic ($\langle a \rangle$) slip (Fig. 10A; Kruhl, 1996), and prismatic sub-grain boundaries that are offset by rhombohedral sub-grain boundaries (Fig. 10B). Microcline is common, and has locally recrystallised to form 0.2-mm-scale, polygonal sub-grains (Fig. 10C). Plagioclase grains commonly exhibit undulose extinction and they have incipient kink-bands, with recrystallisation to form fine ($<$0.1-mm-scale) sub-grains occurring in narrow bands across the crystals. K-feldspar crystals also exhibit undulose

Fig. 8. Photograph of high P_f residual magmatic fluids from the Woodstock Monzogranite (at right) concentrated to form a dyke that intrudes the adjacent granite sheets. View is to the WSW and hammer handle is approximately 40 cm long.

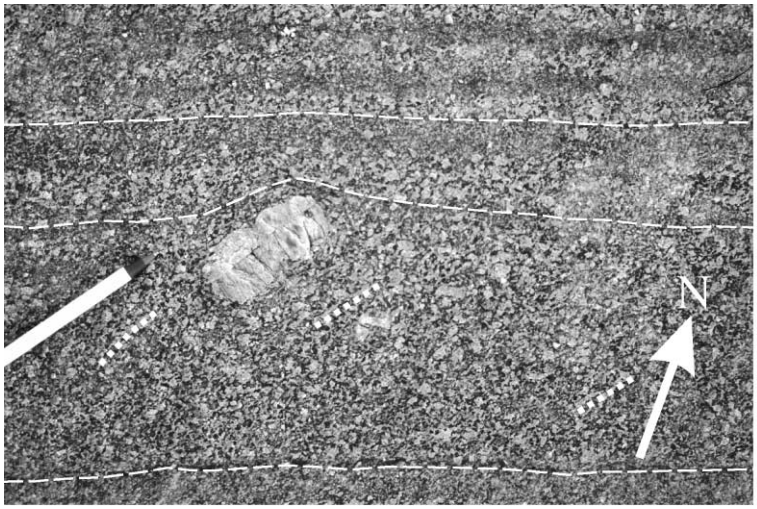

Fig. 9. Photograph of a 5-cm-long K-feldspar grain enveloped by schlieric layers (highlighted by dashed white line) in the Woodstock Monzogranite. Note the apparent flattening of the schlieric layering against the upper left side of the feldspar grain. Common K-feldspar phenocrysts are also aligned parallel to the ~ENE-trending D_c schlieric layering. The pen is oriented parallel to the solid-state S_d foliation defined by elongate quartz aggregates (highlighted by dotted white line), which strikes ~NNE. The arrow points to the north.

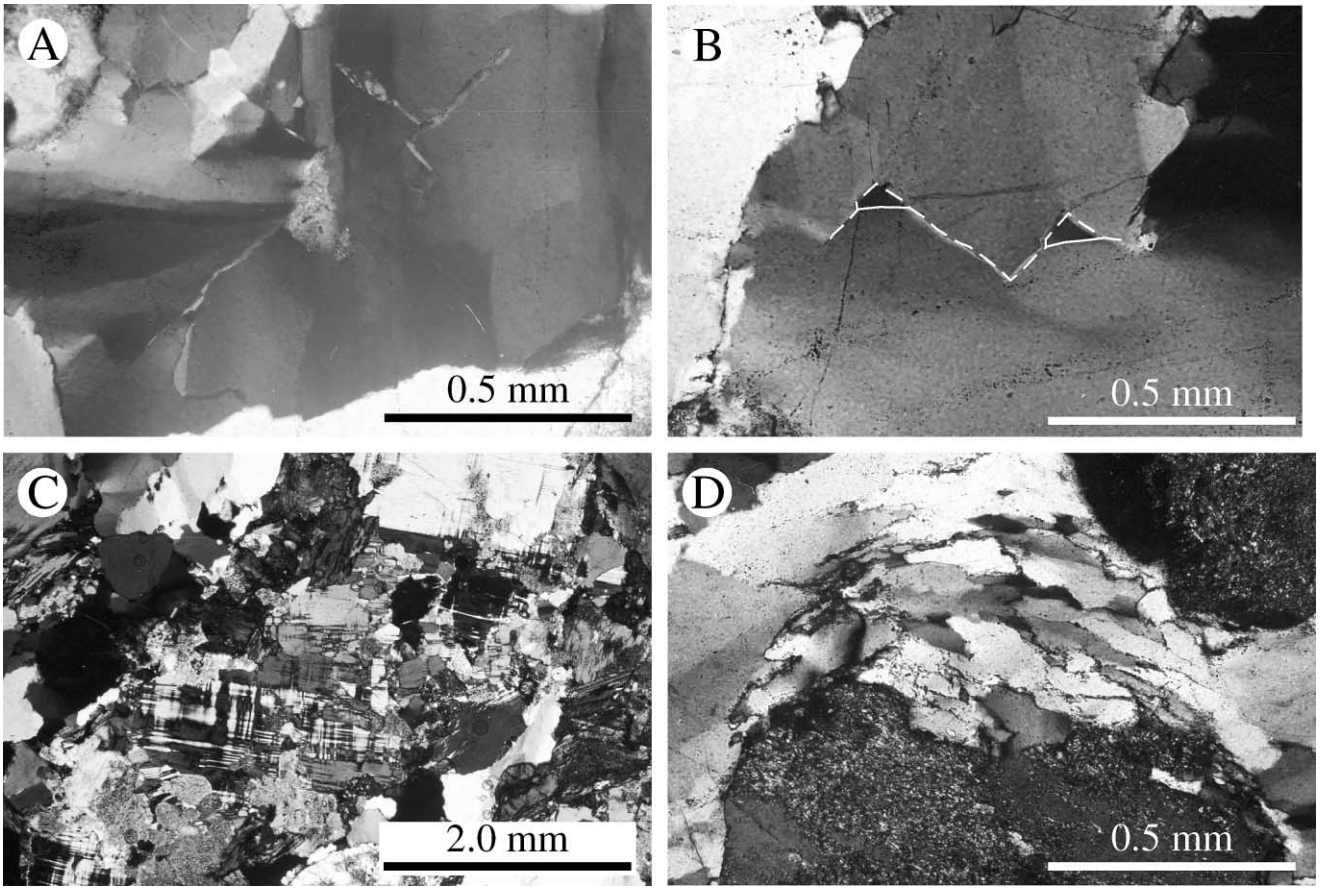

Fig. 10. Photomicrographs to show textures within the Woodstock Monzogranite and granitic sheets. (A) Quartz in the granitic sheets exhibit a 'checkerboard' pattern of sub-grain boundaries to suggest ⟨a⟩ and ⟨c⟩ slip (cross polarised light). (B) Quartz in the granitic sheets with prismatic sub-grain boundaries (highlighted by dashed white line) overprinted by rhombohedral sub-grain boundaries (highlighted by full white line; cross polarised light). (C) Microcline in the monzogranite (same outcrop as the 070°-trending granitic sheets containing the imbricated and rotated blocks) that is re-crystallised (cross polarised light). (D) Quartz ribbons apparently stretched around a feldspar grain in the Woodstock Monzogranite (cross polarised light).

Table 1
Compositional data for the gneissic xenoliths, monzogranite and granite sheets of the Woodstock pluton

	MP97-317A Gneissic xenolith	MP97-317B Gneissic xenolith	MP97-317C Gneissic xenolith	MP97-317H Monzogranite	MP97-317I Monzogranite	MP97-317J Monzogranite	MP97-317L Monzogranite	MP97-317R Monzogranite	MP97-317M Granite sheets	MP97-317N Granite sheets	MP97-317O Granite sheets
Major oxides (wt %)											
SiO_2	71.70	70.36	70.66	71.26	73.03	70.07	71.89	69.35	73.70	73.08	74.22
TiO_2	0.29	0.38	0.32	0.39	0.23	0.48	0.29	0.49	0.23	0.28	0.15
Al_2O_3	15.02	15.12	15.1	14.22	14.16	14.53	13.91	14.66	13.56	13.84	13.81
Fe_2O_3	2.45	3.2	2.86	2.2	1.25	2.98	2.13	3.15	1.90	2.1	1.21
MnO	0.04	0.05	0.06	0.03	0.02	0.05	0.03	0.04	0.03	0.04	0.02
MgO	0.68	0.77	0.78	0.66	0.4	0.69	0.56	0.82	0.36	0.43	0.25
CaO	3.21	3.4	3.28	1.87	1.84	1.91	1.3	2.26	1.51	1.83	1.38
Na_2O	4.59	4.34	4.64	3.81	3.81	3.97	3.59	3.88	3.76	4.02	3.75
K_2O	0.98	1.2	1.08	4.15	3.96	3.86	4.65	3.74	3.82	3.18	4.25
P_2O_5	0.08	0.13	0.1	0.09	0.04	0.14	0.07	0.15	0.05	0.07	0.03
SO_3	0.02	0.02	0.02	0.01	0.01	0.03	0.01	0.02	0.01	0.01	0.01
LOI	0.68	0.81	0.6	0.88	0.82	0.77	0.94	0.91	0.74	0.72	0.66
Total	99.72	99.77	99.48	99.54	99.56	99.48	99.35	99.44	99.66	99.59	99.72
Trace elements (ppm)											
Ba	373	399	304	1767	1820	1437	1118	1729	834	715	852
Rb	95	143	93	130	114.5	184	153	122	127	111	128
Sr	170	177	176	310	331	240	143	289	129	140	120
Cs	b.l.d.	b.l.d.	b.l.d.	b.l.d.	b.l.d.	b.l.d.	b.l.d.	b.l.d.	b.l.d.	b.l.d.	10.5
Pb	14.5	14.5	18.5	28	25	25	30	24.5	24.5	22	27
Th	17	17	17.5	20.5	7.5	27.5	24.5	25	21	19	9.5
U	b.l.d.	b.l.d.	b.l.d.	3	b.l.d.	b.l.d.	b.l.d.	b.l.d.	b.l.d.	b.l.d.	b.l.d.
Zr	144	257	198	212	133	b.l.d.	200.5	248	161	185	98
Hf	5.5	7.5	5.5	5.5	5.5	7	6	7	6	5	4.5
Nb	b.l.d.	b.l.d.	b.l.d.	b.l.d.	b.l.d.	3	b.l.d.	3	b.l.d.	b.l.d.	b.l.d.
Y	12.5	9.5	12.5	5	b.l.d.	8	5.5	27.5	b.l.d.	4.5	b.l.d.
La	18	37	35.5	61	23.5	76.5	57	71	53	0	15.5
Ce	34.5	73	49	85	35	106.5	80	85.5	50	0	37.5
V	15	28.5	24	21	5.5	29	5	32	8.5	0	10.5
Cr	b.l.d.	b.l.d.	b.l.d.	b.l.d.	b.l.d.	b.l.d.	b.l.d.	b.l.d.	6	b.l.d.	b.l.d.
Co	82.5	55	73.5	68	86	113	98	86	84	85	129
Ni	b.l.d.	b.l.d.	b.l.d.	b.l.d.	b.l.d.	b.l.d.	b.l.d.	b.l.d.	b.l.d.	b.l.d.	b.l.d.
Cu	b.l.d.	b.l.d.	b.l.d.	b.l.d.	b.l.d.	b.l.d.	b.l.d.	6.5	b.l.d.	b.l.d.	b.l.d.
Zn	64	76.5	74	62	37.5	83	66	88	53	54	29.5
Ga	17.5	18.5	17.5	17	15	19	17.5	19	17	17.5	15
Cl	20	40.5	46	75	64	67	71	83	60	61	81

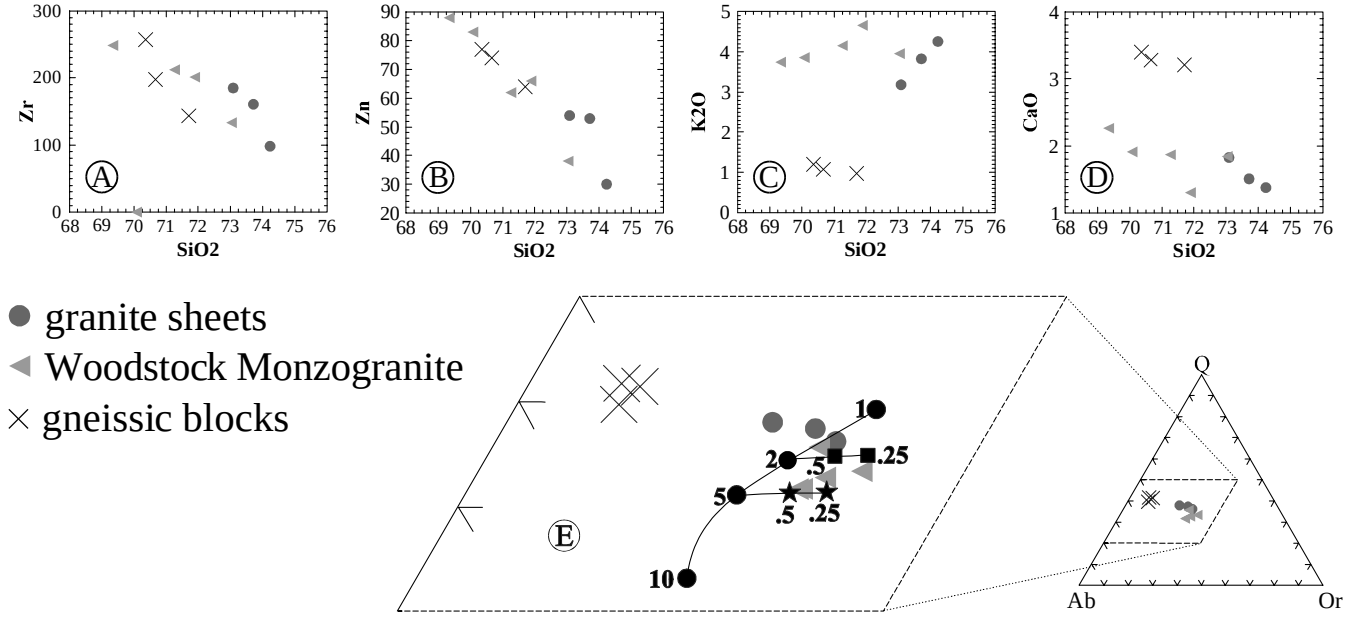

Fig. 11. Geochemistry of the different phases of the Woodstock pluton. (A) to (D) Harker diagrams of selected elements. (E) Ternary plot of normative quartz (Q), albite (Ab) and orthoclase (Or) showing the minimum melt compositions at varying pressures (black filled circles) and H_2O undersaturation. Filled squares are the 2 kbar data and filled stars are the 5 kbar data (Johannes and Holtz, 1996). See text for discussion.

extinction, with some grains having incipient kink-bands, similar to that observed in the plagioclase. The quartz grains have common undulose extinction and they are often flattened to produce quartz ribbons with irregular, serrated edges (Fig. 10D). Apart from the flattened quartz that can be correlated to the mesoscopic S_d quartz ribbons, none of these microstructures can be related to a specific phase of deformation.

4. Geochemistry

The Woodstock Monzogranite, sheets and gneissic xenoliths, have been analysed using standard XRF techniques at the University of Newcastle. The geochemical data are presented in Table 1. The high field strength and transition elements (HFSE and TE, respectively) in the granite sheets have lower abundances relative to the host monzogranite (Fig. 11A and B). In both the granite sheets and the monzogranite, these elements decrease with increasing SiO_2, with the sheets having consistently higher SiO_2 abundances (Fig. 11A and B). The gneissic xenoliths have similar SiO_2, HFSE and TE abundances to the monzogranite, with HFSE and TE also decreasing with increasing SiO_2. Nonetheless, the xenoliths have distinctly low K_2O and high CaO (Fig. 11C and D), indicating the two are not related.

Elements that enter the feldspar lattice (e.g. K_2O and CaO) have similar abundances in both the sheets and host monzogranite (Fig. 11C and D). K_2O increases and CaO decreases with increasing SiO_2 in the granite sheets, whereas the monzogranite has relatively constant K_2O and CaO abundances (although one sample with ~72% SiO_2 has higher K_2O and lower CaO than the general trend; Fig. 11C and D). On the Q–Ab–Or ternary plot (Fig. 11E), the granite sheets trend towards the 1–2 kbar eutectic at $a_{H2O} \sim 1$, the monzogranite compositions cluster around the 2 kbar eutectic for $a_{H2O} \sim 0.5$, and the gneissic blocks cluster away from the eutectic. The geochemistry of the granite sheets (i.e. the decreasing HFSE, TE, and CaO, and increasing K_2O, with increasing SiO_2) suggests that the compositional variation is controlled by either partial melting or crystal fractionation.

The ternary plot (Fig. 11E) shows the compositions of the granite sheets trending towards the 1–2 kbar eutectic (Johannes and Holtz, 1996), suggesting that the sheets crystallised from a magma with crystal fractionation controlling their variation. This contrasts with the monzogranite compositions that form a cluster and do not trend towards the eutectic (Fig. 11E), indicating that their geochemical variation does not result from significant crystal fractionation. Instead, the relatively constant K_2O (Fig. 11C) suggests that K-feldspar accumulation is controlling the variation, an interpretation that is supported by the K-feldspar phenocrysts in the monzogranite.

5. Discussion

5.1. Sheeting into active shear zones

The imbricated gneissic xenoliths within the D_c sheeted granites (Fig. 5) are interpreted to have undergone rotation during shearing to align perpendicular to the shortening direction (e.g. Hanmer and Passchier, 1991; Simpson,

1998). The blocks have either been front- or back-rotated (depending on initial block orientation), with their final orientation suggesting the shortening direction was ~ESE–WNW. Based on the ~40° obliquity between the ~ENE-trending sheets and shortening direction, the blocks are interpreted to have been rotated and aligned during dextral shearing.

The centimetre-scale granite sheets were pinched against the northwest side of the blocks, before being drawn and attenuated over the end of the xenoliths. They were then asymmetrically draped over the northeast side of the block to produce a fold-like geometry (Fig. 5). Vernon (1986), described similar geometries from flow layering deflected around microphenocrysts in lava flows. It was found that the layers were compressed against the side facing the shortening direction and deflected around the end of the phenocryst. After curling around the end of the phenocryst, the layers were drawn into an area of relative expansion to produce a fold-like geometry (see Fig. 3 of Vernon, 1986). The sheet asymmetry also suggests a dextral sense of shear. The absence of a foliation in the enveloping granite sheets, particularly those attenuated against the rigid blocks, suggest they were magmatic during shearing.

The 'spiral' gneissic xenolith is interpreted to have been 'wrapped' by its enclosing sheets during rotation (Fig. 6). The innermost granite sheets were folded as the xenolith and conjoined sheets were rotated within the shear zone. Continued emplacement of later (outer) granite sheets into the developing spiral caused progressive truncation of the earlier-formed sheets. Nonetheless, these sheets were also folded and truncated as rotation and sheet emplacement continued. Only the youngest sheets were not rotated, and are aligned concordantly with the main ENE-direction of the zone. None of these sheets show evidence for foliation development and therefore were magmatic during rotation.

The folds of the 'spiral' xenolith are similar to those that develop within spiral porphyroblasts as inclusion trails (Passchier and Trouw, 1996) and around rotated phenocrysts in lava flows (Vernon, 1986). These folds form during simple shear when the enveloping layers are 'dragged' around with a rotating rigid block and moved into a zone of relative expansion (Vernon, 1986). With greater strain, the layering becomes increasingly attenuated, eventually becoming discontinuous around the xenoliths. Vernon (1986) demonstrated that the fold closures adjacent to the phenocrysts will point in the direction of relative rotation, which implies that the 'spiral' xenolith has undergone clockwise rotation during dextral shearing. The folds also indicate a rheological contrast between a rigid block and a more ductile host (Van Den Driessche and Burg, 1987), suggesting the granite sheets were magmatic during shearing.

The minor sinistral shear zone in the 'spiral' (X in Fig. 6) is interpreted as a high strain band that developed between the limbs during fold tightening (Van Den Driessche and Burg, 1987), rather than an extensional shear band, as this would have the same sense of bulk slip as the shear zone (Hanmer and Passchier, 1991). The non-foliated granite vein in the small shear zone suggests the sheets were not completely crystallised, even during this late stage of dextrally shear-induced clockwise rotation.

The 'comet' xenolith is interpreted as a block that was entrained within a flowing magma sheet. As the host layer contains abundant independant evidence for flow (e.g. schlieren and the dimensional alignment of K-feldspars without recrystallisation textures), it is considered unlikely that the block remained stationary during magma flow. Therefore, it is proposed that both were moving, with the xenolith having a slower velocity relative to the granite magma. The relatively symmetrical tail consisting of discrete magma sheets (Fig. 7), implies that opposite shear acted on both sides of the block and it was not rotating. This resulted in the formation of the tail in a magmatic pressure shadow 'behind' the block, with an inferred southwesterly direction of flow.

The combined evidence from the gneissic xenoliths is that they were carried as rigid blocks in a flowing magma. Some xenoliths are imbricated, others complexly rotated, still others developed comet-like tails. The sense of imbrication and rotation is clockwise, consistent with dextral shearing. This demonstrates that sheeting occurred by repeated injection of small magma increments into an active dextral shear zone.

5.2. Structural evolution in the Woodstock Monzogranite

The Woodstock Monzogranite was emplaced coevally with regional sinistral transpression at ca. 2930 Ma (Zegers et al., 1996; Nelson, 1998; Van Kranendonk and Collins, 1998). Xenolith trains in the pluton were folded into moderately, south-plunging kiilometre-scale F_a synforms with sub-vertical, NNE-trending axial planes (Fig. 2). The hinge zones of folded xenoliths have been intruded by the monzogranite (Fig. 3A and B), suggesting syn-magmatic deformation. A pervasive, sub-vertical, NNE-trending foliation defined by the alignment of euhedral to subhedral K-feldspar (Fig. 3C) is oriented sub-parallel to the axial plane of the folds (Fig. 2), and interpreted to be a magmatic foliation based on the criteria of Paterson et al. (1989). Furthermore, the healing of fractured K-feldspar phenocrysts by quartz (Fig. 3D) indicates that silicate melt was present during deformation.

The geometry of the D_a structures suggest that the ca. 2930 Ma local strain regime can be determined. The F_a axial planes and pervasive ~NNE-trending axial planar S_a foliation typically develop sub-perpendicular to the principal shortening direction (Price and Cosgrove, 1990), suggesting that it was oriented ~ESE–WNW. The general symmetry of the folds and the absence of asymmetric features (e.g. mineral tiling; Blumenfeld and Bouchez, 1988) within S_a suggests that the pluton was undergoing pure shear at this stage, with strain homogeneously

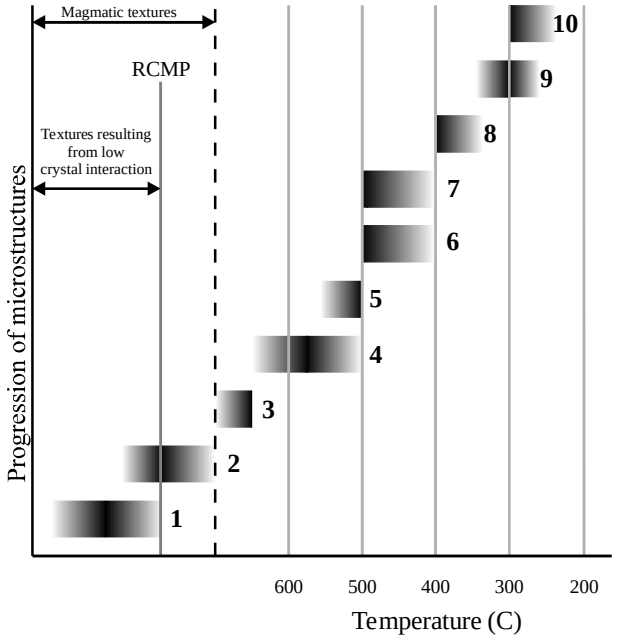

Fig. 12. The relation between temperature and the microtextures preserved within the granite sheets and Woodstock Monzogranite: (1) the mesoscopic mineral alignment would have occurred when the crystal fraction was relatively low and the minerals were able to rotate without significant interaction between grains (Fernandez and Barbarin, 1991; Vigneresse et al., 1996). RCMP refers to the threshold (Tribe and D'Lemos, 1996), where increasing crystal fraction will result in progressive mineral interaction and the onset of solid-state deformation textures; (2) fractured alkali feldspars healed by quartz that is optically continuous with an external quartz grain, suggesting deformation while there was still silicate fluids present, and therefore super-solidus temperatures (also see Fig. 3D); (3) some quartz grains have 'checkerboard' pattern sub-grain boundaries indicating deformation in the high quartz field, suggesting that $T > 650$°C (Kruhl, 1996); (4) rhombohedron sub-grain boundaries suggests deformation in the low quartz field at amphibolite facies temperature (Kruhl, 1996); (5) microcline development suggests that alkali feldspars were deformed at $> \sim 500$°C (Shelley, 1993); (6) plagioclase and microcline recrystallisation indicates deformation at <500°C (Passchier and Trouw, 1996); (7) undulose extinction (weakly developed) in plagioclase indicate upper Greenschist facies (Passchier and Trouw, 1996) and temperatures of $< \sim 500$°C; (8) The kinking of feldspars indicate temperatures of <400°C (Passchier and Trouw, 1996); (9) the development of fine quartz sub-grains, suggest that temperature of deformation was ~300°C (Passchier and Trouw, 1996); (10) the flattened quartz ribbons that have not recrystallised suggest that deformation was continuing at $< \sim 300$°C (Passchier and Trouw, 1996).

distributed. Although no lineations were measured in the Woodstock Monzogranite, the sub-horizontal lineations in the MSZ/LWSC (Van Kranendonk and Collins, 1998; Zegers et al., 1998) suggest that σ_1 was regionally sub-horizontal.

In contrast to the D_c sheets, the D_b granite sheets contain gneissic xenoliths that are symmetric or do not exhibit a consistent asymmetry. Furthermore, these sheets have pinch and swell geometries (Fig. 4), suggesting extension in the plane of intrusion. Nonetheless, the minerals are not aligned, nor are the granites recrystallised in the extension direction, again indicating that deformation occurred in the magmatic state. The absence of asymmetric xenoliths implies that the D_b granite sheets are not simple shear zones and may represent high strain zones that developed during fold tightening in a pure-shear environment (Van Den Driessche and Burg, 1987).

Following emplacement of the D_b granite sheets, the D_c magma-dominated dextral shear zone developed in the pluton. This zone is characterised by the imbricated-, spiral- and comet-like geometries of the xenoliths, all of which indicate transport in a magma.

Adjacent to the ENE-trending D_c shear zone, the host monzogranite contains two oblique foliations defined by dimensionally aligned K-feldspar crystals. The dominant foliation trends ENE and is defined by the 'matrix' K-feldspar. The minor foliation trends NNE and is defined by 5-cm-long K-feldspars (Fig. 9). The lack of recrystallisation associated with these two foliations suggests that they formed under magmatic conditions. The foliations are also confined to within <100 m of the shear zone, suggesting that they are related to D_c deformation.

The obliquity between the two foliations suggests that the mineral alignment occurred during non-coaxial deformation, with alignment of the 'matrix' K-feldspars in the shear transport direction and rotation of the larger grains perpendicular to the shortening direction (Blumenfeld and Bouchez, 1988), indicating dextral shear. The geometry of the schlieren wrapping around the large phenocrysts (Fig. 9) is similar to the geometry of the imbricated blocks within the shear zone (Fig. 5), and the asymmetry is consistent with a dextral sense of shear zone. These textural relations indicate that the D_c shear zone developed while the host pluton was incompletely crystallised.

The coaxial nature of deformation in the localised D_b zones, and the non-coaxial nature of the D_c zones indicates that they do not form a conjugate pair of shear zones. They also indicate that the pluton was subjected to heterogeneous deformation and strain partitioning during crystallisation.

The zones of sheeted granite are overprinted by the pervasive, ~NNE-trending sub-solidus S_d foliation (Fig. 2). This indicates that, at this stage, strain was again homogeneously distributed throughout the pluton. The development of S_d sub-parallel to S_a (Fig. 2B) suggests that the shortening direction had not significantly changed during deformation of the pluton.

The microstructures preserved in the granite sheets and host monzogranite, and the temperature conditions they reflect, are summarised in Fig. 12. Overall, they indicate a transition from super-solidus textures (i.e. interlocking igneous texture), through high-temperature sub-grain boundary development, to moderate-temperature microcline development and feldspar recrystallisation, and ultimately to low-temperature textures preserved in quartz. Based on the textures, it is interpreted that the granite sheets were emplaced as magmas during deformation, which continued throughout crystallisation and cooling.

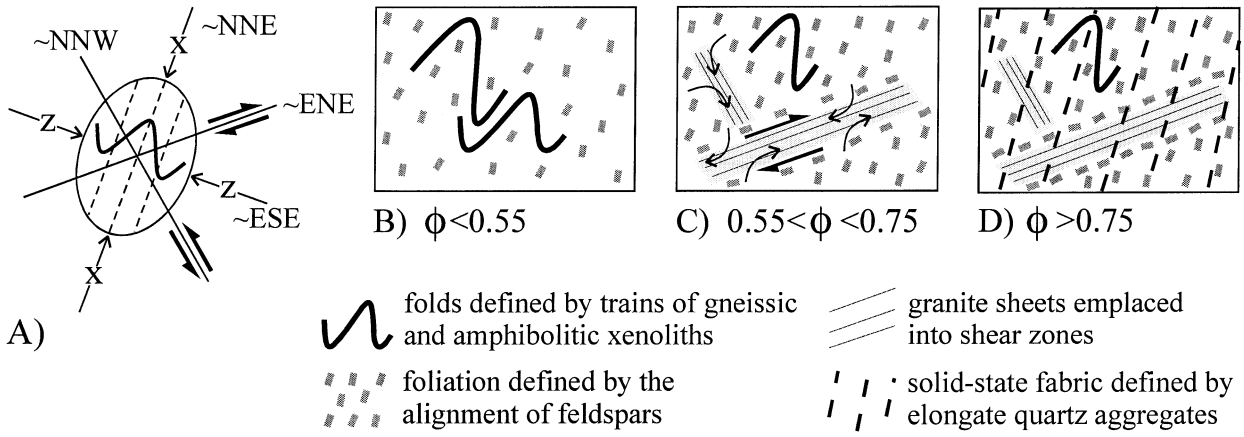

Fig. 13. Diagram showing the development of the contrasting structures in the Woodstock pluton as the crystal fraction increased. (A) Qualitative strain ellipse showing the relation of the structures to the regional principal strains. The dashed lines represent the regional, axial planar, sub-solidus S_d. (B) Folding of the xenolith trains and development of the NNE-trending axial planar S_a during Newtonian fluid behaviour. (C) Transient brittle failure during shear thickening to produce the NNW-trending D_b granite sheets and the ENE-trending D_c dextral shear zone (with local K-feldspar phenocryst realignment). (D) Development of the NNE-trending solid-state S_d (defined by quartz aggregates) during Newtonian behaviour.

5.3. A model of structural development during progressive crystallisation

The sequential development of structures in the Woodstock Monzogranite can be related to the changing magma rheology as the crystal fraction (Φ) increased during crystallisation, summarised in Fig. 13. On emplacement, the syn-kinematic magma underwent shortening at low crystal fractions ($\Phi < 0.3$–0.55; Fernandez and Barbarin, 1991; Vigneresse et al., 1996) to produce kilometre-scale D_a structures (Fig. 13B). The pervasive rotation and alignment of K-feldspar phenocrysts during D_a suggests it was a crystal-poor Newtonian fluid (Paterson et al., 1989), where strain was homogenously distributed throughout the magma. This foliation developed sub-parallel to the fold axial plane and sub-perpendicular to the regional shortening direction (Fig. 13A; e.g. Price and Cosgrove, 1990).

As crystallisation continued (0.3–$0.55 < \Phi < 0.75$), interactions between minerals became more frequent and the magma formed a permeable framework that behaved as a non-Newtonian viscous material. Under low strain rates, the crystals flowed relative to each other and the magma body behaved as a fluid (Fernandez and Barbarin, 1991; Vigneresse et al., 1996). However, increased strain rates, or greater P_f, caused the magma to behave as a transient solid and undergo brittle failure (i.e. 'strain thickening' of Smith (1997, 2000)). The increased P_f may be the result of deformation-enhanced compaction reducing pore space in the matrix of the host monzogranite, thereby increasing the pore pressure (Rutter, 1997). As well as promoting transient brittle failure, the P_f gradients would cause interstitial melt to move into the relatively low pressure shear zones (Fig. 13C; discussed in Section 5.4), thereby contributing melt to the ~NNE-trending granite sheets parallel to S_b and the ~ENE-trending D_c dextral shear zone (Figs. 2 and 13C).

Adjacent to the D_c shear zone, K-feldspar phenocrysts in the host mozogranite were rotated and aligned parallel to the shear zone, with simple shear producing mineral imbrication and *S/C* style fabrics (Fig. 9), even though all the deformation occurred under magmatic conditions. Mineral alignment probably occurred by grain boundary sliding (see Fig. 5e of Park and Means, 1996), which is required for non-Newtonian behaviour at the higher crystal fractions ($0.55 < \Phi < 0.75$).

At very high crystal fractions ($\Phi > 0.75$), the minerals formed a closely packed network, causing the pluton to behave as a solid (Newtonian behaviour; Fernandez and Barbarin, 1991; Vigneresse et al., 1996). The strain within the crystalline pluton was effectively homogenously distributed, generating the penetrative, ~NNE-trending sub-solidus S_d fabric (Fig. 13D). Microstructures in the granite sheets (e.g. kinking of K-feldspars and undulose extinction and sub-grain development in quartz) demonstrate that sub-solidus deformation continued to low temperatures (~300°C; Fig. 12).

5.4. Shearing, magma pressure and the granite sheets

The angle (~40°) between the magma-filled dextral D_c shear zone and the shortening direction (perpendicular to S_a and S_d) allows inferences to be made about P_f within the crystallising magma. As the inferred shortening direction is similar to the NW–SE oriented σ_1 proposed by Van Kranendonk and Collins (1998), it is suggested that deformation was essentially coaxial, with local partitioning of strain to form the shear zone. Based on Mohr stress analysis, the calculated 80° angle between conjugate fractures (2θ) is too high for hybrid extensional shear failure (requiring $2\theta < 45°$), which occurs when the fracture dilates during shearing (Price and Cosgrove, 1990). Instead, the angular

relation between the shear zone and σ_1 supports hybrid compressional shear failure. This occurs when $2\theta > 45°$ and induces compression upon the shear plane (Price and Cosgrove, 1990). However, the repeated injection of granite sheets indicates transient dilation along the shear plane, suggesting that the melt pressure was periodically sufficiently high to 'jack' open the shear zone.

An inferred high magma pressure in the pluton is supported by 'dewatering' structures (Fig. 8), where melt segregated from monzogranite layers to form the sharp edged, funnel-shaped dyke that cuts the adjacent granite sheets (Fig. 8). Reorientation of schlieric layering adjacent to the end of the dyke suggests that magma pressure exceeded the yield strength of the sheets, causing it to fracture, allowing ingress from the overpressured monzogranite layer.

It therefore appears that high P_f within the pluton may have contributed to shearing and the generation of the granite sheets. However, the virtual restriction of gneissic xenoliths suggests that a significant proportion of the magma was derived from another source that contained gneisses.

The xenoliths are remnants of older orthogneisses, which occur as screens and marginal phases within the Yule Granitoid Complex and probably also exist below the Woodstock pluton. The gneissic blocks were most probably transported from deeper crustal levels to form the xenolith-rich zones in some granite sheets. Saint Blanquat et al. (1998) has shown that differential stresses imposed during transpressional deformation can cause 'tectonic overpressuring', resulting in increased magma pressure. Combined with buoyancy, this results in vertical pressure gradients and the efficient upward flow of magma within strike-slip structures. The presence of dewatering structures and virtual confinement of gneissic xenoliths to the D_b and D_c granite sheets within the host pluton, are consistent with more efficient upward flow in these magma-dominated shear zones.

5.5. Other considerations

The Woodstock pluton provides evidence for coeval magma emplacement and transfer. The absence of migmatitic textures (e.g. Sawyer, 1999) in the homogeneous Woodstock pluton suggests that it represents a crystallising magma that had segregated from its source and been emplaced at a higher structural level. In contrast, the zones containing numerous S_b and S_c sheeted granites are fractures or shears that developed within the pluton during crystallisation of the host. These zones became local sites of low P_f, resulting in rapid, focussed flow of underlying, but rising granitic magma. As such, they are transfer zones, and provide excellent evidence for magma migration mechanisms at upper crustal levels.

The foliations developed in the Woodstock Monzogranite are either oblique, or unrelated to those in the adjacent country rocks. To the northeast, the pluton is separated from the greenstones by the ca. 2930 Ma MSZ/LWSC that locally trends NW–SE (Fig. 1; Van Kranendonk and Collins, 1998). The greenstones southeast of the pluton form part of a roof pendant associated with doming at ca. 3240 Ma (Fig. 1; Van Kranendonk, 1997). They are highly strained ($L \gg S$) with mineral elongation and rodding lineations that plunge shallowly to the southwest (Van Kranendonk, 1997). Directly adjacent to the pluton contact, the greenstones have a schistose fabric which is concordant to the NE-trending margin. The schist is intruded by local, concordant granite sheets and therefore should be coeval with D_{a-d}. However, it is consistently 20–30° oblique to the S_{a-d} foliations in the pluton. Consequently, foliations within and outside the pluton that have widely varying orientations and appear kinematically unrelated, are still coeval.

6. Conclusions

The Woodstock Monzogranite in the Pilbara Craton of Western Australia is a syn-kinematic pluton, which underwent rheological changes during cooling and crystallisation. The result was a complex interplay between rheology and structural development.

1. At high melt fractions (low Φ) the magma behaved as a Newtonian fluid, early formed K-feldspar phenocrysts were able to rotate freely and align perpendicular to the regional shortening direction during D_a deformation.
2. As crystallisation continued ($0.3–0.55 < \Phi < 0.75$), a rigid crystal network developed, which behaved as a non-Newtonian body. This resulted in D_b and D_c strain partitioning and the initiation of shearing, which was oriented oblique to S_a and the regional shortening direction. These developed into magma transfer sites, where magma flowed as centimetre-scale sheets. Adjacent to the D_c shear zone, feldspar phenocrysts aligned during granular flow to form a tiling mineral foliation aligned parallel to the granite sheets.
3. The pervasive solid-state S_d foliation developed perpendicular to the regional shortening direction, indicating deformation occurred at higher crystal contents ($\Phi > 0.75$). At this stage the crystallising pluton had the rheology of a Newtonian solid.
4. The sequential down-temperature development of magmatic and sub-solidus structures described in this study highlight the complexities that may be encountered in the field. The study demonstrates that a lower temperature (i.e. sub-solidus) foliation will not necessarily be parallel to, or continuous with, the syn-tectonic magmatic foliations in the pluton. Consequently, oblique magmatic and solid-state foliations may not represent distinct deformation events as they can form sequentially during a single deformation event during crystallisation of a granite pluton.

Acknowledgements

Research was supported by a University of Newcastle Research Scholarship (M. Pawley). M. Van Kranendonk and A. Melville are thanked for assistance in the field. The Geological Survey of Western Australia provided logistical support for fieldwork. The manuscript benefited from discussions with J.-L. Vigneresse. P. Barbey and G. Solar are thanked for thorough reviews.

References

Bickle, M.J., Bettenay, L.F., Chapman, H.J., Groves, D.I., McNaughton, N.J., Campbell, I.H., Laeter, J.R.d., 1989. The age and origin of younger granitic plutons of the Shaw Batholith in the Archaean Pilbara Block, western Australia. Contributions to Mineralogy and Petrology 101, 361–376.

Bickle, M.J., Bettenay, L.F., Chapman, H.J., Groves, D.I., McNaughton, N.J., Campbell, I.H., Laeter, J.R.d., 1993. Origin of the 3500–3300 Ma calc-alkaline rocks in the Pilbara Archaean: isotopic and geochemical evidence from the Shaw Batholith. Precambrian Research 60, 117–149.

Blumenfeld, P., Bouchez, J.-L., 1988. Shear criteria in granite and migmatite deformed in the magmatic and solid state. Journal of Structural Geology 10, 361–372.

Brown, M., Solar, G.S., 1998. Granite ascent and emplacement during contractional deformation in convergent orogens. Journal of Structural Geology 20, 1365–1393.

Buick, R., Thornett, J.R., McNaughton, N.J., Smith, J.B., Barley, M.E., Savage, M., 1995. Record of emergent continental crust ~3.5 billion years ago in the Pilbara craton of Australia. Nature 375, 574–577.

Buttner, S., 1999. The geometric evolution of structures in granite during continuous deformation from magmatic to solid-state conditions: an example from the central European Variscan Belt. American Mineralogist 84, 1781–1792.

Davidson, C., Schmid, S.M., Hollister, L.S., 1994. Role of melt during deformation in the deep crust. Terra Nova 6, 133–142.

Fernandez, A.N., Barbarin, B., 1991. Relative rheology of coeval mafic and felsic magmas: nature of resulting interaction processes and shape and mineral fabrics of mafic microgranular enclaves. In: Didier, J., Barbarin, B. (Eds.). Enclaves and Granite Petrology. Elsevier, Amsterdam, pp. 263–275.

Grujic, D., Mancktelow, N.S., 1998. Melt-bearing shear zones: analogue experiments and comparison with examples from southern Madagascar. Journal of Structural Geology 20, 673–680.

Hanmer, S., Passchier, C.W., 1991. Shear-sense Indicators: A Review. Geological Survey of Canada.

Hickman, A.H., 1983. Geology of the Pilbara Block and its Environs. Geological Survey of Western Australia, Perth.

Hollister, L.S., Crawford, M.L., 1986. Melt-enhanced deformation: a major tectonic process. Geology 14, 558–561.

Johannes, W., Holtz, F., 1996. Petrogenesis and Experimental Petrology of Granitic Rocks. Springer-Verlag, Berlin.

John, B.E., Stunitz, H., 1997. Magmatic fracturing and small-scale melt segregation during pluton emplacement: evidence from the Adamello Massif (Italy). In: Bouchez, J.L., Hutton, D.H.W., Stephens, W.E. (Eds.). Granite: From Segregation of Melt to Emplacement Fabrics, vol. 8. Kluwer Academic Publishers, Dordrecht, pp. 55–74.

Kruhl, J.H., 1996. Prism- and basal-plane parallel subgrain boundaries in quartz: a microstructural geothermobarameter. Journal of Metamorphic Geology 14, 581–589.

Mahood, G.A., Cornejo, P.C., 1992. Evidence for ascent of differentiated liquids in a silicic magma chamber found in a granitic pluton. Transactions of the Royal Society of Edinburgh: Earth Sciences 83, 63–69.

McCaffrey, K.J.W., 1994. Magmatic and solid state deformation partitioning in the Ox Mountains granodiorite. Geological Magazine 131, 639–652.

McCaffrey, K.J.W., Miller, C.F., Karlstrom, K.E., Simpson, C., 1999. Synmagmatic deformation patterns in the Old Woman Mountains. SE California. Journal of Structural Geology 21, 335–349.

Miller, R.B., Paterson, S.R., 1994. The transition from magmatic to high-temperature solid-state deformation: implications from the Mount Stuart batholith, Washington. Journal of Structural Geology 16, 853–865.

Nelson, D.R., 1998. Compilation of SHRIMP U–Pb Zircon Geochronology Data. Western Australia Geological Survey.

Park, Y., Means, W.D., 1996. Direct observation of deformation processes in crystal mushes. Journal of Structural Geology 18, 847–858.

Passchier, C.W., Trouw, R.A.J., 1996. Microtectonics. Springer-Verlag, Berlin.

Paterson, S.R., Vernon, R.H., Tobisch, O.T., 1989. A review of criteria for the identification of magmatic and tectonic foliations in granitoids. Journal of Structural Geology 11, 349–363.

Pitcher, W.S., Berger, A.R., 1972. The Geology of Donegal: A Study of Granite Emplacement and Unroofing. Wiley-Interscience, New York.

Pons, J., Barbey, P., Dupuis, D., Leger, J.M., 1995. Mechanisms of pluton emplacement and structural evolution of a 2.1 Ga juvenile continental crust: the Birimian of southwestern Niger. Precambrian Research 70, 281–301.

Price, N.J., Cosgrove, J.W., 1990. Analysis of Geological Structures. Cambridge University Press, Cambridge.

Rosenberg, C.L., Handy, M.R., 2000. Syntectonic melt pathways during simple shearing of a partially molten rock analogue (Norcamphor–Benzamide). Journal of Geophysical Research 105, 3135–3149.

Rutter, E.H., 1997. The influence of deformation on the extraction of crustal melts: a consideration of the role of melt-assisted granular flow. In: Holness, M.B. (Ed.). Deformation-enhanced Fluid Transport in the Earth's Crust and Mantle. Chapman & Hall, London, pp. 82–110.

Rutter, E.H., Neumann, D.H.K., 1995. Experimental deformation of partially molten Westerly granite under fluid-absent conditions, with implications for the extraction of granitic magmas. Journal of Geophysical Research 100, 15,697–15,715.

Saint Blanquat, M., Tikoff, B., Teyssier, C., Vigneresse, J.-L., 1998. Transpressional kinematics and magmatic arcs. In: Holdsworth, R.E., Strachan, R.A., Dewey, J.F. (Eds.). Continental Transpressional and Transtensional Tectonics. , pp. 327–340 Geological Society Special Publication 135.

Sawyer, E.W., 1994. Melt segregation in the continental crust. Geology 22, 1019–1022.

Sawyer, E.W., 1996. Melt segregation and magma flow in migmatites: implications for the generation of granitic magmas. Transactions of the Royal Society of Edinburgh: Earth Sciences 87, 85–94.

Sawyer, E.W., 1999. Criteria for the recognition of partial melting. Physics and Chemistry of the Earth 24 (3), 269–279.

Schofield, D.I., D'Lemos, R.S., 1998. Relationships between syn-tectonic granite fabrics and regional PTtd paths: an example from the Gander–Avalon Boundary of NE Newfoundland. Journal of Structural Geology 20, 459–471.

Shelley, D., 1993. Igneous and metamorphic rocks under the microscope: classification, textures, microstructures and mineral preferred orientations. Chapman & Hall, London.

Simpson, C., 1998. Rotated porphyroclast systems in quartzo–feldspathic mylonites. In: Snoke, A.W., Tullis, J., Todd, V.R. (Eds.). Fault-related Rocks: A Photographic Atlas. Princeton University Press, Princeton, pp. 334–339.

Smith, J.V., 1997. Shear thickening dilatancy in crystal-rich flows. Journal of Volcanology and Geothermal Research 79, 1–8.

Smith, J.V., 2000. Textural evidence for dilatant (shear thickening) rheology of magma at high crystal concentrations. Journal of Volcanology and Geothermal Research 99, 1–7.

Thorpe, R.I., Hickman, A.H., Davis, D.W., Mortensen, J.K., Trendall, A.F., 1992. U–Pb zircon geochronology of Archaean felsic units in the

Marble Bar region, Pilbara Craton, Western Australia. Precambrian Research 56, 169–186.

Tribe, I.R., D'Lemos, R.S., 1996. Significance of hiatus in down-temperature fabric development within syn-tectonic quartz diorite complexes, Channel Islands, UK. Journal of the Geological Society, London 153, 127–138.

Van Den Driessche, J., Burg, J.-P., 1987. Rolling structures at large shear strain. Journal of Structural Geology 9, 691–704.

Van Kranendonk, M.J., 1997. Results of field mapping, 1994–1996, in the North Shaw & Tambourah 1:100,000 sheet areas, eastern Pilbara Craton, northwestern Australia. Australian Geological Survey Organisation.

Van Kranendonk, M.J., 1998. Lith-tectonic and structural components of the North Shaw 1:100,000 sheet, Archaean Pilbara Craton. In: Geological Survey of Western Australia Annual Review 1997–98. Geological Survey of Western Australia, pp. 63–70.

Van Kranendonk, M.J., Collins, W.J., 1998. Timing and tectonic significance of Late Archaean, sinistral strike-slip deformation in the Central Pilbara Structural Corridor, Pilbara Craton, Western Australia. Precambrian Research 88, 207–232.

Vauchez, A., Neves, S.P., Tommasi, A., 1997. Transcurrent shear zones and magma emplacement in Neoproterozoic belts of Brazil. In: Bouchez, J.L., Hutton, D.H.W., Stephens, W.E. (Eds.). Granite: From Segregation of Melt to Emplacement Fabrics. Kluwer Academic Publishers, Dordecht, The Netherlands, pp. 275–293.

Vernon, R.H., 1986. A microstructural indicator of shear sense in volcanic rocks and its relationship to porphyroblast rotation in metamorphic rocks. Journal of Geology 95, 127–133.

Vigneresse, J.L., Barbey, P., Cuney, M., 1996. Rheological transitions during partial melting and crystallisation with application to felsic magma segregation and transfer. Journal of Petrology 37, 1579–1600.

Williams, I.S., Collins, W.J., 1990. Granite–greenstone terranes in the Pilbara Block, Australia, as coeval volcano-plutonic complexes; evidence from U–Pb zircon dating of the Mount Edgar Batholith. Earth and Planetary Science Letters 97, 41–53.

Zegers, T.E., 1996. Structural, kinematic and metallogenic evolution of selected domains of the Pilbara granitoid–greenstone terrain: implications for mid Archaean tectonic regimes. PhD thesis, Universiteit Utrecht.

Zegers, T.E., White, S.H., de Keijzer, M., Dirks, P., 1996. Extensional structures during deposition of the 3640 Ma Warrawoona Group in the eastern Pilbara Craton, Western Australia. Precambrian Research 80, 89–105.

Zegers, T.E., Keijzer, M.d., Passchier, C.W., White, S.H., 1998. The Mulgandinnah Shear Zone; an Archean crustal scale strike-slip zone, eastern Pilbara, Western Australia. Precambrian Research 88, 233–247.